Temperature Field and Power Loss Calculation With Coupled Simulations for a Medium-Voltage Simplified Switchgear

Ahmet Efe Şeker[1] , **Bayram Çelik[2]** , **Deniz Yıldırım[3]** , **Egemen Aslan Sakacı[4]** , **Arif Deniz[4]**

[1]Aeronautical and Astronautical Engineering Program, İstanbul Technical University, İstanbul, Turkey
[2]Department of Astronautical Engineering, İstanbul Technical University, İstanbul, Turkey
[3]Department of Electrical Engineering, İstanbul Technical University, İstanbul, Turkey
[4]Gebze Research and Development Center, Siemens, Kocaeli, Turkey

ABSTRACT

The main goal of the present study is to carry out one-way coupled computations of electromagnetics and heat transfer for a simplified version of a switchgear and to reveal the applicability of the computational approach. In our computation, we introduce the joule losses that we obtain from the electromagnetic computations to a thermal solver as heat load. In order to reach the goal, we compare the temperature values that we obtained at eight different measurement points by performing computations and experimental measurements. In general, the distributions of the obtained temperature values are quite similar. The notable difference in the mean values of the obtained temperatures might result from limitations of one-way coupled approach where we have to neglect temperature dependency of the electrical properties during the electromagnetic computations.

Index Terms—Computational fluid dynamics, electromagnetic analysis, eddy current loss, natural convection, switchgear

Corresponding author:
Ahmet Efe Şeker

E-mail:
aefeseker@gmail.com

I. INTRODUCTION

Since the beginning of the use of electricity, switchgears have been used in many sectors. This trend emphasizes the importance of switchgears in electrical distribution. Today, the distribution of electrical energy and its continuity has become a standard of urban life. Increasing demand for electrical energy decreases the total impedance of the grid [1, 2]. Therefore, short circuit current magnitudes increase. The key role of switchgears is to protect the electricity grid while meeting current demand. Today, switchgears can be designed to take on this role. Computer-aided design and computation tools considerably facilitate the design studies of switchgears.

Recently, the number of studies similar to the present study has increased. Radeva et al. made a study for solving coupled electromagnetic and thermal field of a laboratory busbar system using a two-stage approach [3]. A steady-state temperature field was used as the initial condition for a transient simulation. This method has low computational cost since the simulation was performed in two-dimension. Results showed good agreement with measurements and were useful to produce an insight for more complex problems. A comparison study between simplified and advanced approaches on the busbar system of a switchgear was carried out by Bedkowski et al. [4] where variant 1 is the most simple approach and neglects the alternating current effects. Then two different variants were considered with a one-way coupled approach between electromagnetics and computational fluid dynamics (CFD). The former was carried out with an arbitrary temperature and the temperature taken from experiments was used in the latter. Finally, a two-way coupled simulation was carried out by taking into account alternating current, skin and proximity effects. Natural convection effects were employed as boundary conditions. The outputs of the simulations were compared with experimental data showing that computational cost increases as the method gets more complex. Researchers utilized the outputs of the study and conducted another study using a two-way coupled approach between electromagnetics and CFD on a switchgear [5]. Moreover, joint electric resistivity losses were taken into account. Simulations and measurements were performed on switchgears that are naturally ventilated and

have a hermetic enclosure. In order to reduce the number of cells, non-conformal mesh feature was utilized. Researchers aimed to judge the effects of the turbulence model, heat transfer coefficient on external walls, surface emissivity, and joint electric resistivity losses to the thermal performance. As a result, it was concluded that the turbulence model and the heat transfer coefficient on the external walls did not have a significant effect. Radiation was reported as a very important heat transfer mode for the thermal performance of a switchgear. On the other hand, it is not easy to accurately estimate the emissivity, which plays a key role in radiation heat transfer. The employment of joint electrical resistivity losses results in reduction of the average temperature discrepancy in naturally ventilated configurations. However, the average temperature discrepancy was increased in enclosed configurations. The same research group improved its work by focusing on emissivity [6]. A two-way coupled simulation approach and cutcell meshing method were adopted as in the previous study. Two configurations with both ventilated and hermetic enclosures similar to the previous study were simulated. In order to increase the emissivity, a coating layer is added and surface brushing is employed. Although these methods increase heat dissipation, surface brushing is not easy to apply to the system and the coating layer causes additional thermal resistance. The average difference between measured and computed temperatures for naturally ventilated and hermetic enclosure configurations is 11% and 9%, respectively. Therefore, the simulation model is considered as a verified model regarding the modification of cooling capability. It is shown that the high emissivity provides a significant temperature drop in the busbar system. Moreover, the temperature drop in natural ventilated configuration is steeper than hermetic enclosure configuration. Unlike the studies of Bedkowski, natural convection effects can be included in the simulation by modeling outer air. Qu et al. made simplifications on the simulation object in their study [7]. Accordingly, the circuit breaker was modeled as three flat conductors enclosed by a solid cube. Moreover, the busbars which were outside the switchgear were not modeled. Therefore, the influence of the busbars on the surrounding air was not taken into account. One-way coupling between electromagnetics and CFD was adopted and heat transfer by radiation was neglected. Simulation results were compared with measurements and the maximum temperature discrepancy was determined to be as 11 K. Even though one-way coupling was used, the result is remarkable. Recently, studies on switchgear modeling are in the rise. One of those studies, which was on the optimization of airflow inside a switchgear, reveals the role of the airflow for cooling enhancement [8]. In another study, the authors focus on the development of the flow and temperature fields of a switchgear capsule via lattice Boltzmann method, which is a nonconventional CFD method that is based on kinetic theory [9].

Besides numerical simulations based on commercial software, there are a significant amount of studies performed with in-house solvers for analyzing switchgears and their components. The study by Gramsch et al. is a good example for such studies [10]. In this study, researchers put forward a method called the thermal network method (TNM). This method can be used for the design of power devices such as switchgears. Dong et al. used TNM to examine the temperature rise of a gas-insulated medium-voltage switchgear [11]. The authors validated the method by comparing their results with the experimental measurements. It is concluded that TNM is a highly efficient method for the thermal management of gas-insulated switchgears. Singh et al. made a study that combined TNM and CFD [12]. They performed initial analyses by using TNM and CFD

separately. Then, they combined TNM and CFD and compared their results with previously obtained ones. They reported that the combination of TNM and CFD matched the experimental results better. The thermal network method has been adopted for modeling more advanced problems such as thermal performance evaluation of connected systems after its successful applications [13]. According to the aforementioned success of the approach, TNM has a significant contribution to the literature.

Studies in the literature include detailed information for the understanding of switchgear thermal management. The present study differs from the studies in the literature by mainly concerning current transformer (CT), airflow, and experimental studies. In the present study, lamination definition in the core of the CTs was adopted. Moreover, power losses caused by CTs' secondary windings were applied as heat load to the cores of the CTs. To the best of knowledge, the present study is unique in terms of considering experimental and computational studies together and providing their comparison for a switchgear. Therefore, the present study fills the gap regarding the evaluation of electromagnetic measurements. Besides, unlike the studies in the literature, two sets of temperature rise experiment data are used. In our previous study, we obtained temperature distribution and compared it with the experimental result [14]. Outer air volume was included in the computation domain, in both electromagnetic (EMAG) and CFD analyses. Heating due to the CT secondary windings was not considered. The temperature distribution was compared with just one experimental result.

This study aims to go beyond the results of the previous study [14]. In accordance with this purpose, the computational domain was modeled more realistically. In addition to that, meshing strategy and boundary conditions were reconsidered. Instead of the outer frame, boundary layer meshes were applied to the busbars. Tetrahedral elements were used in the computational domain excluding the boundary layer. Outer air volume is not used in CFD computations. Instead, the natural convection effects were applied as boundary conditions.

II. EXPERIMENTAL STUDIES

In this study, electrical and thermal experiments were conducted, and the results obtained from those experiments were used in

Fig. 1. Test object.

EMAG and CFD analyses. Electrical experiments consist of direct current (DC) resistance experiment and alternating current (AC) power experiment whereas thermal experiment is conducted to determine temperature rise. In our preliminary study, only one temperature rise experiment data was used [14]. Here, one more temperature rise experiment was made. Thus, two sets of temperature rise experiments are available for evaluating temperature distributions. Rated frequency and rated current are 50 Hz and 830 A, respectively. The test object used in the experiments is shown in Fig. 1. A schematic of the test object that shows the experimental setup is shown in Fig. 2.

A. DC Resistance Measurement Experiment

The aim of the experiment is to determine the DC resistance of the test objects' components. Resistance measurement was made with Chauvin Arnoux CA6250 micro ohmmeter. The device is given a test current of 10 A to the current path and then the voltage drop between the connection points was measured. Since the measured voltage drop and the value of the given test current are known, the resistance can be calculated using Ohm's law. Each measurement has been performed according to the relevant current path. For full circuit resistance, the beginning points of the current paths are TC_{R_1}, TC_{S_1}, TC_{T_1}, and the end point is the TC_{S_8}, which is the
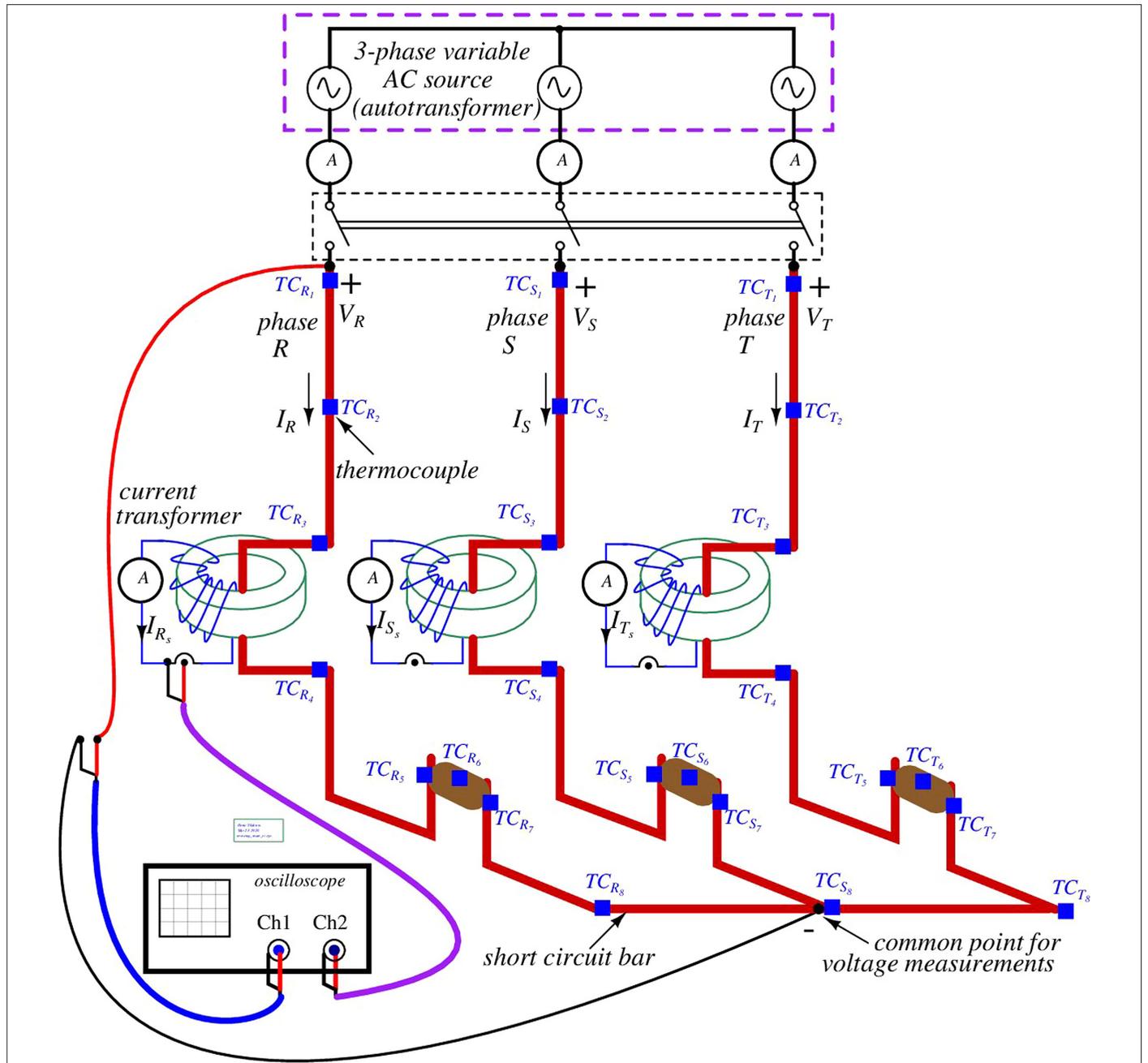

Fig. 2. Experimental setup scheme.

TABLE I. DC RESISTANCE MEASUREMENT PARAMETERS AND MEASURED RESISTANCE VALUES

Phase	Full Circuit (mΩ)	CT Poles (mΩ)		Secondary Windings (mΩ)			Tulip Contacts (mΩ)
R	98.90 @ $TC_{R1} - TC_{R8}$	39.20 @ $TC_{R3} - TC_{R4}$	Bottom	221.50	Top	299.70	4.00 @ $TC_{R5} - TC_{R7}$
S	80.60 @ $TC_{S1} - TC_{S8}$	31.40 @ $TC_{S3} - TC_{S4}$		215.50		289.60	5.30 @ $TC_{S5} - TC_{S7}$
T	86.70 @ $TC_{T1} - TC_{T8}$	29.60 @ $TC_{S3} - TC_{S4}$		223.60		293.50	5.40 @ $TC_{T5} - TC_{T7}$

CT, current transformer.

midpoint of the star point. The resistance between the poles of the CTs was also measured between the third and fourth points in each phase. These resistances correspond to resistances between the ends of the primary windings of the CTs. Each CT has two cores and there are two secondary windings wound on these cores. The resistances between the ends of these secondary windings were measured. Each phase has one tulip contact. These contacts touch the busbars from the front and back, where the resistances between these touch points were measured between the fifth and

seventh points in each phase. DC resistance measurement parameters and measured resistance values are shown in Table I, whereas the measurement points can be seen in Fig. 2. The resistance values obtained for the secondary windings were used in the CFD analysis. Using these resistance values, joules losses were estimated. These losses were applied to the secondary windings of the CTs as heat load in CFD simulations.

B. AC Power Measurement Experiment
This experiment aims to measure the AC power loss in each phase conductor and thereby the total power loss in the circuit can be calculated. Electromagnetic results can be verified using the experimental results. The experiment was performed at the rated frequency and rated current of the test object. AC power losses of the busbar system were measured by analyzing AC voltage and current waveforms with Tektronix TPS2024 oscilloscope. Secondary winding current was also measured with Fluke 337 AC clamp meter. AC power loss measurement values are given in Table II. The turn ratio of the CTs used in the simplified model is 250. In other words, total power loss is 250 times the power loss of 3 CTs. Accordingly, the total power loss in the circuit is calculated as 238.5 W.

TABLE II. AC POWER LOSS MEASUREMENT VALUES

Phase	Voltage Drop (mV)	Secondary Winding Current (A)	Secondary Power (mW)
R	314 @ $TC_{R1} - TC_{R8}$	3.3	469
S	245 @ $TC_{S1} - TC_{S8}$	3.3	262
T	287 @ $TC_{T1} - TC_{T8}$	3.3	223
Total			954

TABLE III. TEMPERATURE RISE EXPERIMENTS—MEASURED TEMPERATURES

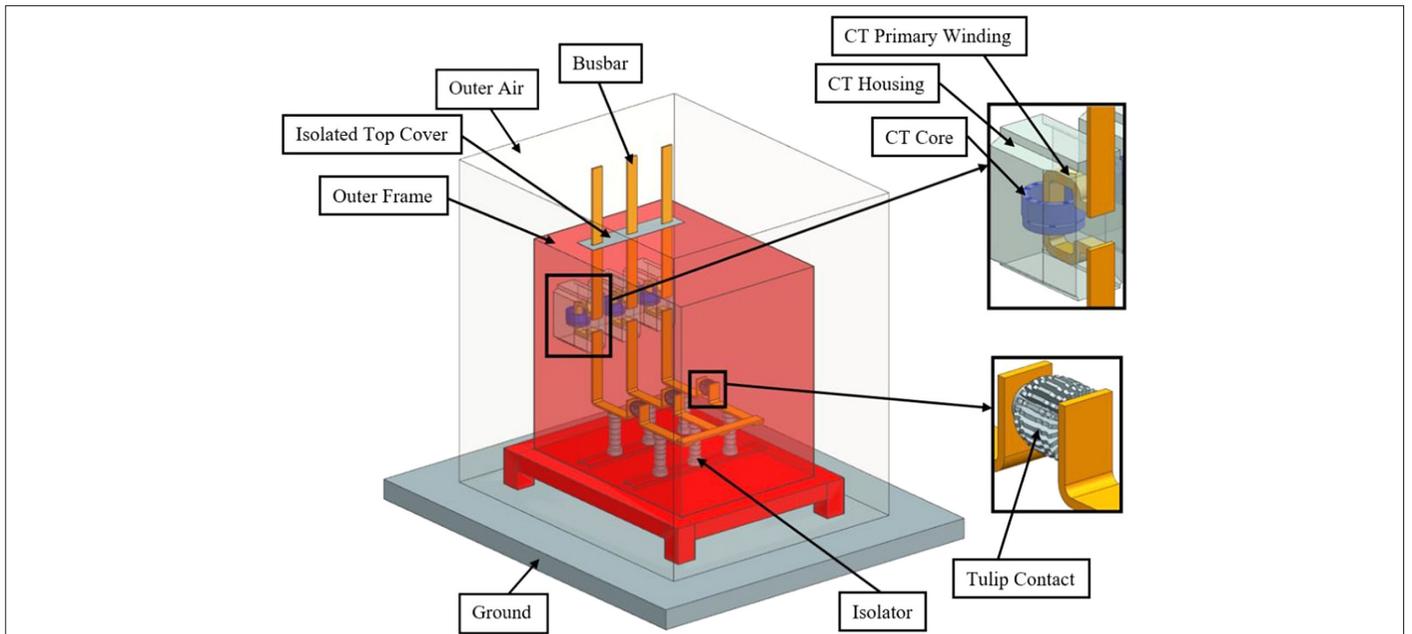| Measurement Point	Limit Temperature (°C)	Measured Temperature (°C) First Set	Measured Temperature (°C) Second Set	Measurement Point	Limit Temperature (°C)	Measured Temperature (°C) First Set	Measured Temperature (°C) Second Set
TC_{R_1}	-	52.60	60.8	TC_{R_5}	75.00	67.00	69.2
TC_{S_1}	-	52.40	64.5	TC_{S_5}	75.00	67.00	69.6
TC_{T_1}	-	55.40	59.5	TC_{T_5}	75.00	65.50	67.9
TC_{R_2}	-	58.90	64.1	TC_{R_6}	75.00	66.90	69.4
TC_{S_2}	-	58.30	66.9	TC_{S_6}	75.00	67.20	69.8
TC_{T_2}	-	58.80	62.3	TC_{T_6}	75.00	65.90	67.7
TC_{R_3}	75.00	73.00	71.6	TC_{R_7}	75.00	66.80	69.4
TC_{S_3}	75.00	72.90	72	TC_{S_7}	75.00	65.30	67.9
TC_{T_3}	75.00	69.50	66.4	TC_{T_7}	75.00	63.60	66.5
TC_{R_4}	75.00	69.20	75.7	TC_{R_8}	-	67.30	69.2
TC_{S_4}	75.00	68.60	75.3	TC_{S_8}	-	67.50	69.1
TC_{T_4}	75.00	64.80	71	TC_{T_8}	-	66.50	69.1

Fig. 3. Simulation model.

C. Temperature Rise Experiment

Temperature rise experiment is a type test for switchgears. The aim is to determine the temperature rise of the components compared to the ambient temperature. Experiments were conducted at rated frequency and rated current. Preparation for the experiment and execution was made in accordance with the directive prepared by Siemens. This directive is prepared according to IEC 62271-1: 2017 standard [15]. The experiment termination criterion depends on the temperature change of the test object. The experiment is terminated if the temperature change is less than 1 Kelvin per hour. The voltage drop is measured before and after the experiment. The difference between these measurements must not exceed 20%. Temperature rise experiments were performed in two sets. The ambient air temperature was 24°C and 27°C for the first and second experiment, respectively, because there is no air conditioning device available in the experiment room to set ambient temperature to a fixed value. Ambient temperature used in the EMAG and CFD analyses is taken from the first experiment. Results of the simulations and results of the experiments were shown in Table III.

III. COMPUTATIONAL MODEL

In order to extend the findings of preliminary results obtained by Seker et al. [14], the computational model was redesigned as shown in Fig. 3. Bottom supports of the outer frame and the concrete ground were added to the simulation model [14]. Boundary conditions were reconsidered to model the physics of the problem more realistically.

In EMAG analysis, the role of the outer air volume was to bind the computational domain. Moreover, it was required for modeling surrounding air in CFD analysis. In this way, natural convection effects were considered. Convective boundary conditions were applied to the top surfaces of the busbars. The reason for this was to model the cables connected to busbars. Computational cost is reduced by excluding outer air volume from CFD analysis. Natural convection

effects are now implemented to the system as a new boundary condition where natural convection is taken into account. Fixed temperature values were applied to the top surfaces of busbars instead of modeling cables. Simulations were performed in one-way coupled manner as in the previous study [14]. At first, eddy current loss density distribution (ECLD) is calculated with EMAG solver. Then, the calculated losses are applied as heat load to the system for CFD computations. One-way coupled simulation requires identical meshes for computations of the power losses and temperature fields. Therefore, the mesh used in EMAG analysis should be employed in CFD analysis where boundary conditions for EMAG and CFD analyses are illustrated in Fig. 4. Simulations were performed with coarse (C), medium (M), and fine (F) meshes for a convergence check. Assigned material properties for the switchgear components can be seen in Table IV.

A. Electromagnetic Analysis

Electromagnetic analysis was carried out with the commercial finite element solver, Magnetics for NX [16]. It simplifies and solves Maxwell's equations according to the problem type [17]. In this study, the air volume surrounding the switchgear is only used in EMAG analysis. On the boundary of the air domain, magnetic wall conditions (i.e., null magnetic vector potential tangent component) are enforced. Voltage and current sources were defined on the top surfaces of the busbar. Current with a 120° phase angle was defined on the R and S phase. Zero voltage is defined in phase T to direct the current flow as it should. Galvanized steel and iron are ferromagnetic materials which are used in the computational model. Ferromagnetic materials have nonlinear magnetic permeability and yet a linear value can be used for magnetic permeability value. This can be done by considering the linear portion of the magnetization or hysteresis curve. In this study, linear magnetic permeability values were used for both galvanized steel and iron. Magnetization curve for galvanized steel is taken from a reference material [18], and for iron, it is taken from the manufacturer's technical data sheet [19]. Magnetic permeability values for galvanized steel and iron were calculated as 1923 H/m and 80 000 H/m, respectively. In difference with
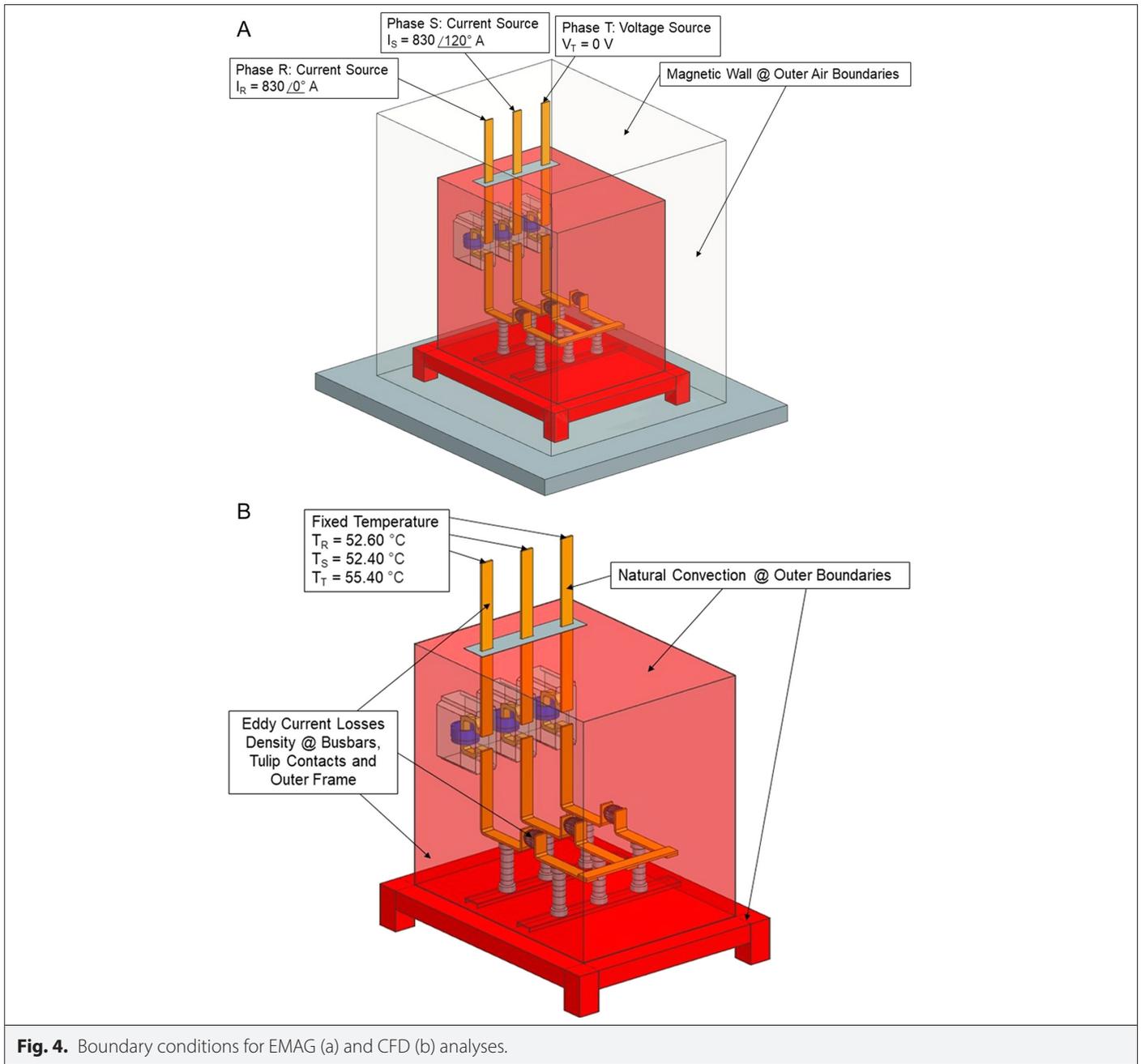
Fig. 4. Boundary conditions for EMAG (a) and CFD (b) analyses.

TABLE IV. MATERIALS OF THE COMPONENTS

Material	Component
Electrolytic copper	Busbar, CT primary winding, tulip contact
Epoxy	Isolator, CT housing
Iron	CT core
Galvanized steel	Outer frame
Unsaturated polyester glass mat	Isolated top cover
Concrete	Ground
Air	Air inside the simplified switchgear, environment air

CT, current transformer.

the previous study, cores of the CTs were added to the simulation model. In accordance with reality, these cores are modeled as laminated in the computational model. This is not a CAD operation but a definition in the computational model. The result of the EMAG analysis is ECLD of the switchgears' components. Eddy current losses density in the cores of the CTs is expected as negligible order because lamination reduces the eddy current losses significantly. Presuming that the conducting volume of both cores is the same, eddy current loss in a laminated core composed of k laminations is k^2 times lower than in a solid core [1]. Eddy current losses density was used as the heat source input for CFD analysis. Magnetics for NX does not cover the calculation of the eddy current losses on coils [17]. Therefore, the heat generated on the secondary coils of the CTs was calculated manually. For this purpose, secondary coil resistance and current values were used.
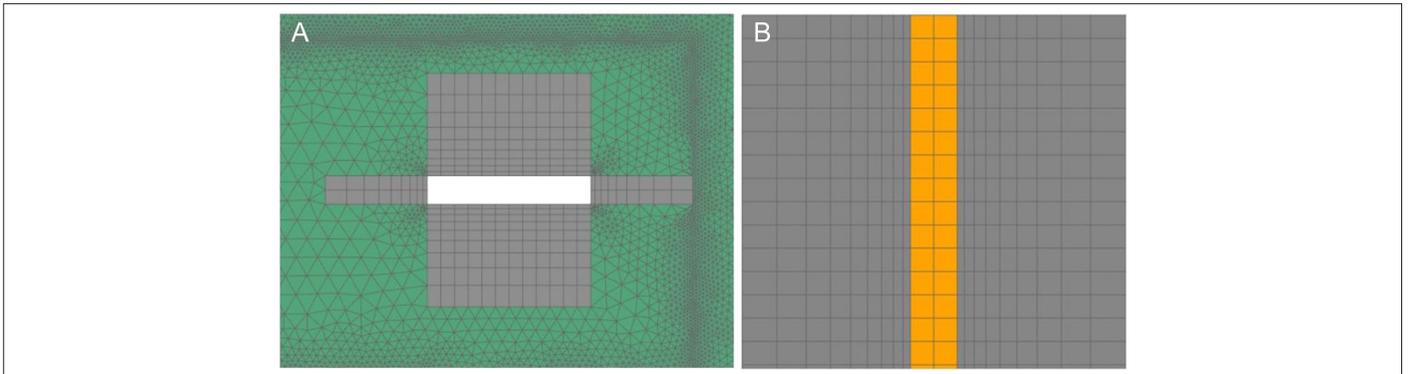
Fig. 5. Top (a) and side (b) views of the boundary layer elements near the busbar.

B. Computational Fluid Dynamics Analysis

Computational fluid dynamics computations were performed by using Siemens Simcenter 3D Thermal/Flow solver. This solver is based on the finite volume method. Governing equations considered in the solver are conservations of mass, momentum, and energy. Computational fluid dynamics computations are performed in a two-way coupled fashion for thermal and flow analyses. However, the coupling between EMAG and CFD is one-way. Coupling was made between thermal- and buoyancy-driven flow analyses. Natural convection boundary conditions were applied to the outer frame's outer surfaces. These boundary conditions represent the effect that causes cooling of the outer frame. Boussinesq approximation was used for applying natural convection effects to

the computational domain. This approximation considers the effect of the density gradient on the buoyancy force, which moves the fluid [20, 21]. The boundary conditions take the characteristic length in vertical and horizontal directions. The top surfaces of the busbars are set to be at a fixed temperature. These values are taken from the first temperature rise experiment. No-slip wall boundary condition is applied on the solid surfaces. Eddy current losses density is introduced to the system as heat load. The heat caused by the secondary coils was distributed uniformly on the cores of the CTs. This approximation was considered appropriate as secondary coils wrap to the bodies of the cores. Since there is no external flow source, the flow is buoyancy driven. Wall regions have high velocity and temperature gradients. Boundary layer meshes were adopted to resolve these gradients with high resolution. Top and side views of the boundary layer cells near the busbar are shown in Fig. 5. Velocity boundary layer (VBL) was generated properly by considering the value of the Grashof number. The characteristic length of the busbar was determined by considering free flow paths without obstacles. The top cover blocks the air to flow freely. Therefore, the length between
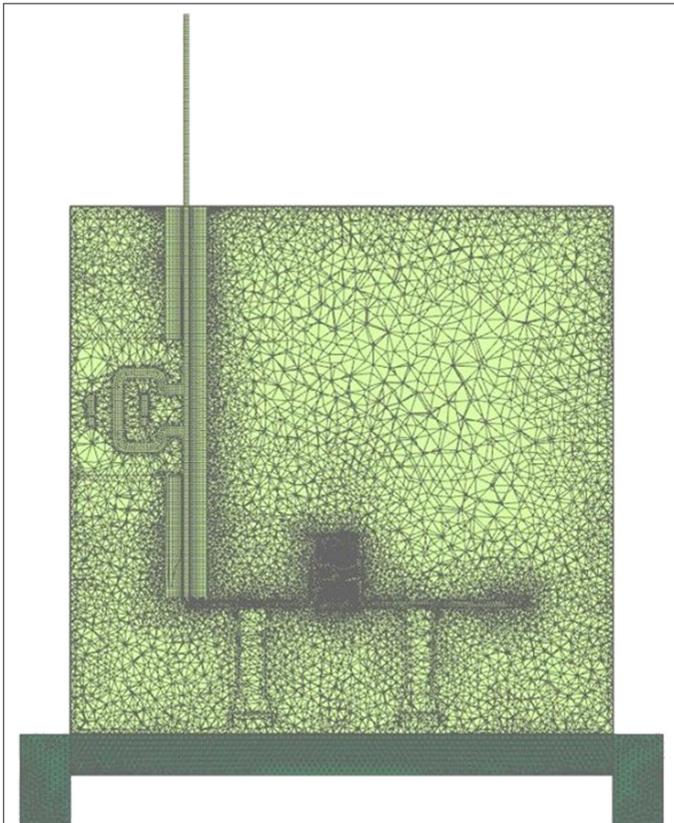

Fig. 6. Fine mesh for CFD analysis.

TABLE V. TOTAL EDDY CURRENT LOSSES

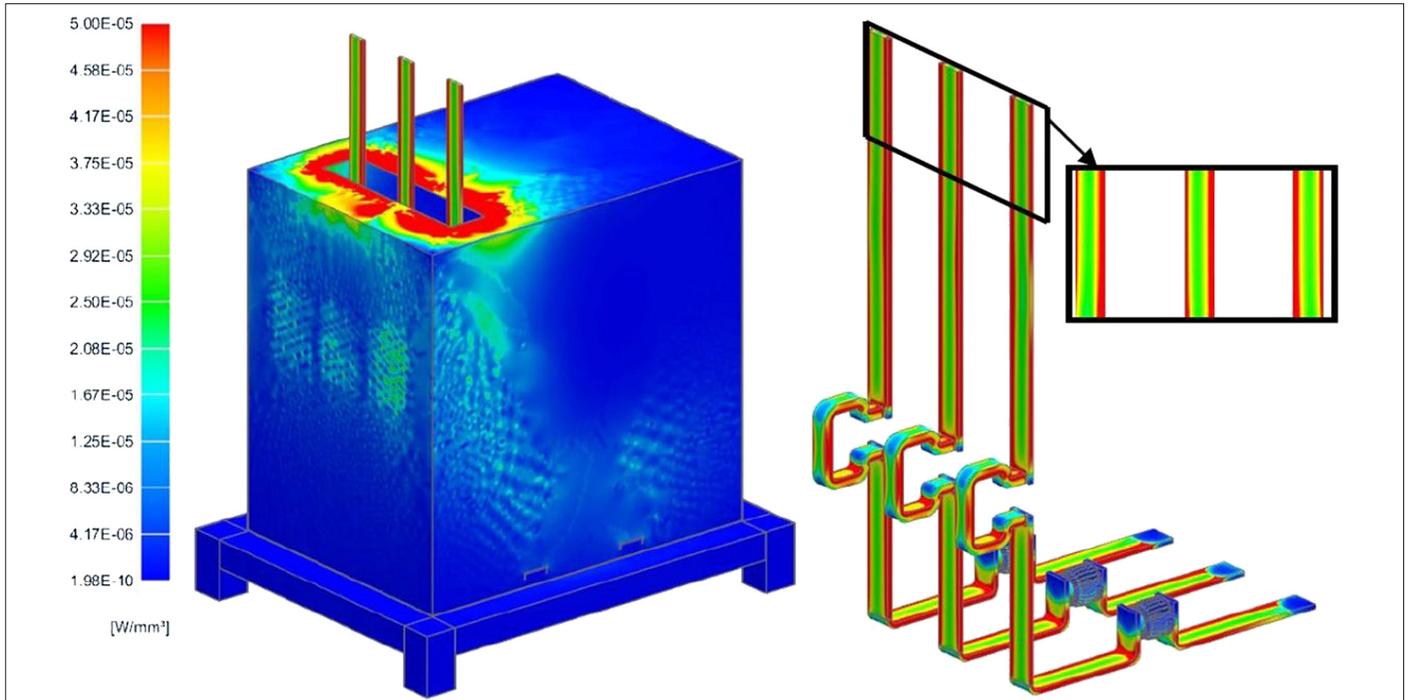| Mesh	Coarse	Medium	Fine	
Number of elements	1 389 381	1 744 768	4 057 189	
Number of nodes	250 757	339 737	1 118 143	Maximum Error Percentage
Component	Eddy Current Loss (W)			
Tulip contact—S	1.27	1.28	1.28	0.78
Tulip contact—R	1.32	1.33	1.33	0.75
Tulip contact—T	1.26	1.27	1.27	0.79
Busbar—S	48.57	48.69	48.78	0.25
Busbar—R	49.76	49.81	49.86	0.10
Busbar —T	48.15	48.33	48.43	0.37
Short circuit busbar	8.47	8.42	8.50	0.94
Outer frame	52.76	53.31	53.80	1.03
Total	211.56	212.44	213.25	0.41

Fig. 7. Eddy current losses density distribution of the computational model.

measurement points second to third is considered as characteristic length. Prandtl number indicates the ratio of the VBL thickness to thermal boundary layer (TBL) thickness. Thus, TBL thickness can be calculated utilizing Prandtl number. According to experiments, the temperature interval of the computational domain is approximately 52–76°C. Prandtl number of the air is less than 1 for such a temperature range. Since the TBL is thicker than the VBL, boundary layer mesh was generated according to TBL thickness. In this way, both velocity and temperature gradients can be resolved with the desired accuracy. The fine mesh used in the CFD analysis is shown in Fig. 6.

IV. RESULTS

In the first step of both EMAG and CFD analyses, a coarse mesh was used. Then cell sizes of the mesh were reduced gradually. This strategy is adopted to provide a grid-independent solution. In EMAG analysis, conductive parts show large variations of the current density magnitude. Accordingly, the number of elements of conductive parts increased in each mesh refinement step. Analyses are repeated until the difference between consecutive analyses goes below 2%. When the difference is negligible, the result is considered as grid-independent. The size of the cells for the region of air has a major
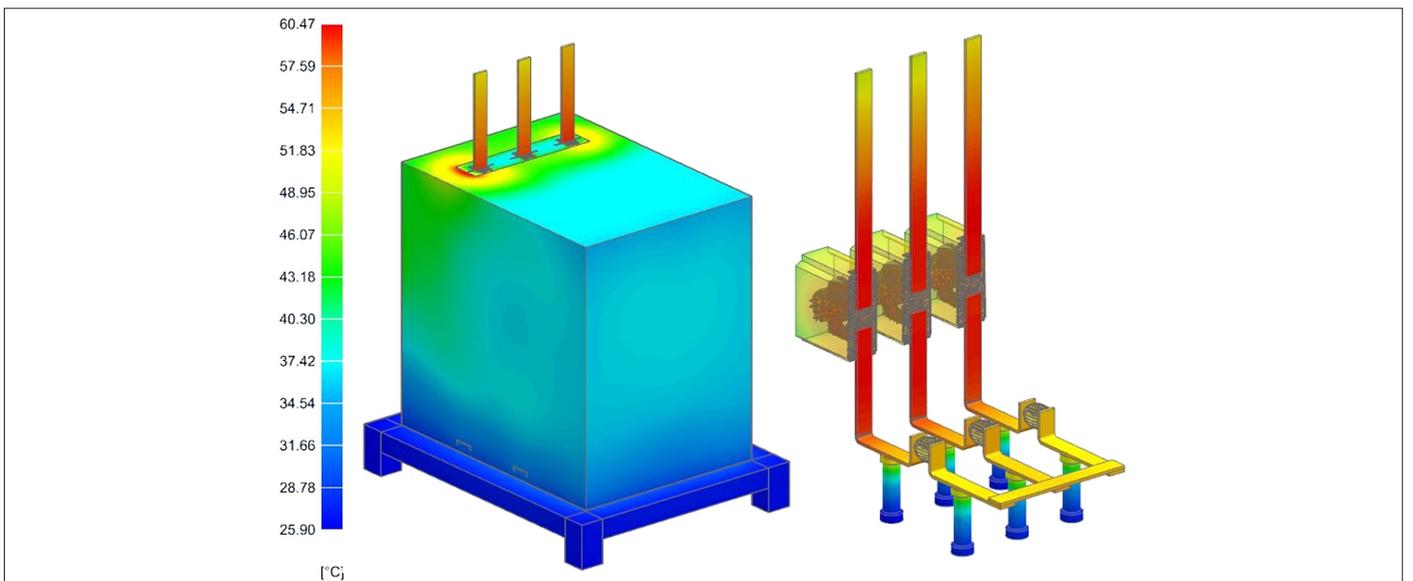

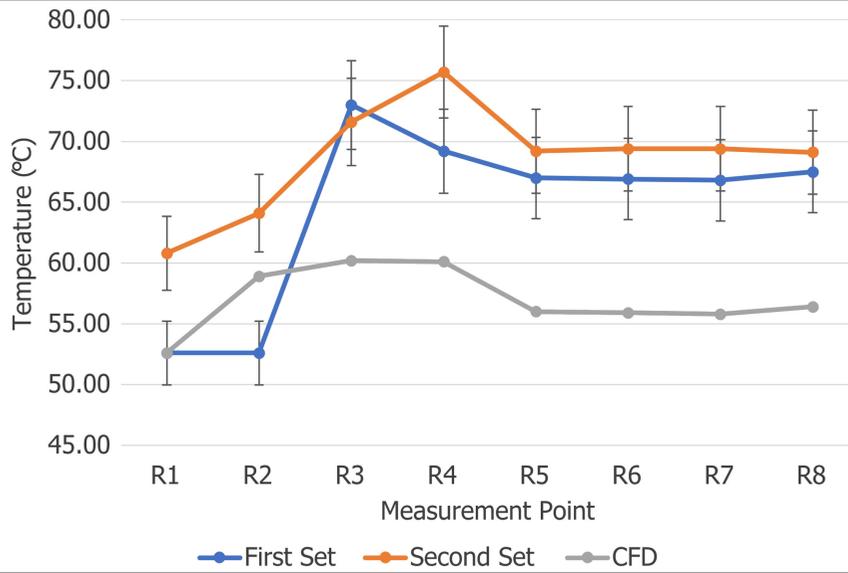**Fig. 8.** Temperature distribution of the computational model.

Fig. 9. Measured and calculated temperatures of the components—R.

effect on the natural convection. Therefore, mesh resolution of the air was increased for obtaining a grid-independent CFD solution. Boundary layer mesh was set to maximum feasible resolution in order to resolve high gradients. Accordingly, boundary layer mesh remains fixed in all meshes. Eddy current losses density values were obtained with the meshes of the conductive parts. Therefore, these meshes were conserved while increasing resolution. As in EMAG analysis, when the difference is negligible, the result is considered to be mesh-independent.

Total eddy current losses (TECL) of each component were calculated with Magnetics for NX, except the coils. Total eddy current losses of the coils were calculated with data in Tables I and II. Accordingly, resistance of the secondary winding and square of the secondary winding current are multiplied for each secondary winding. Summation of these values is the TECL of the coils. Total eddy current losses of

the coils were calculated as 19.81 W. The components of TECL can be seen in Table V. The maximum differences were calculated with (1). Accordingly, the maximum difference between results from different mesh densities is less than 2%. Eddy current losses density values were obtained for each node and can be seen in Fig. 7.

$$\frac{Result_{Coarse,Medium} - Result_{Fine}}{Result_{Fine}} \times 100 \qquad (1)$$

The comparison of the calculated temperatures with different mesh densities is shown in Table VI. The maximum differences were calculated with (1). The maximum difference between results from different mesh densities is less than 2%. The temperature distribution of the computational model can be seen in Fig. 8. Sets of the experiments and the calculated temperature distributions are compared to each other. Comparison plots for each phase were shown
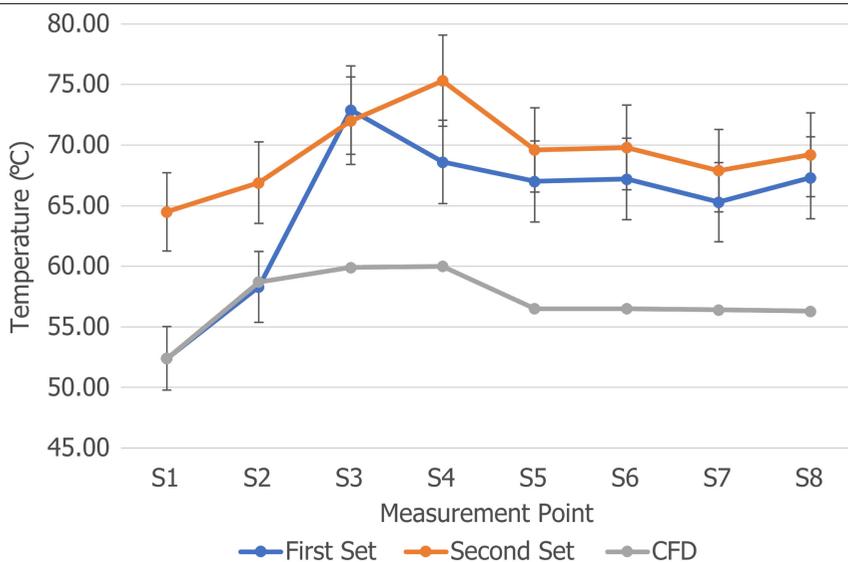

Fig. 10. Measured and calculated temperatures of the components—S.
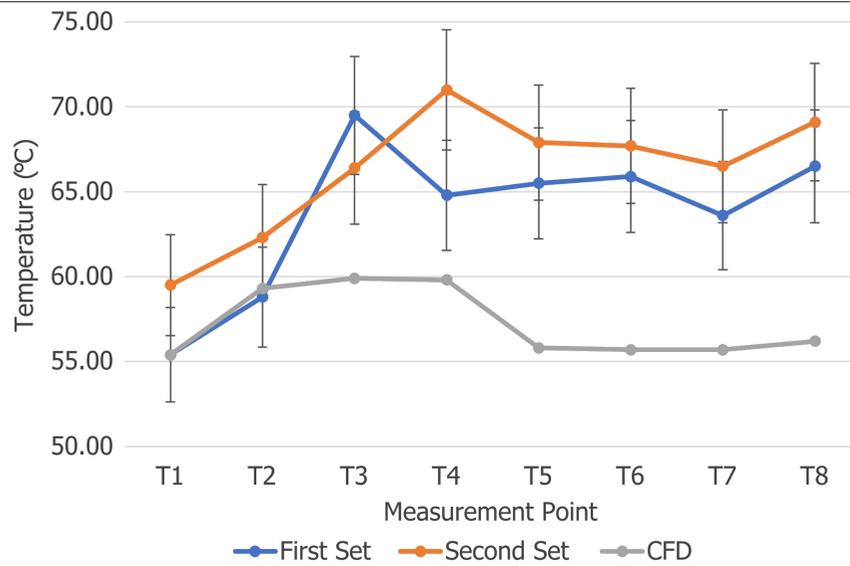
Fig. 11. Measured and calculated temperatures of the components—T.

in Figs. 9-11. The error bars show 5% of error for each set of experiments. Except for the first and the second measurement points, experiments comply with each other with 5% error.

The streamlines colored by the velocity magnitude in the switchgear and its mid-section view can be seen in Figs. 12 and 13, respectively. Progress of velocity profile in the boundary layer is important for interpreting the results. The velocity gradient in the boundary layer can be seen in Fig. 14. Although the air temperature inside the outer frame was not measured with experiment, it was obtained from CFD analyses. Thus, air temperature can be compared with limit temperatures of the components. The temperature contours adjacent to the busbar are shown in Fig. 15. In this figure, the temperature contours adjacent to the busbar are also observable.
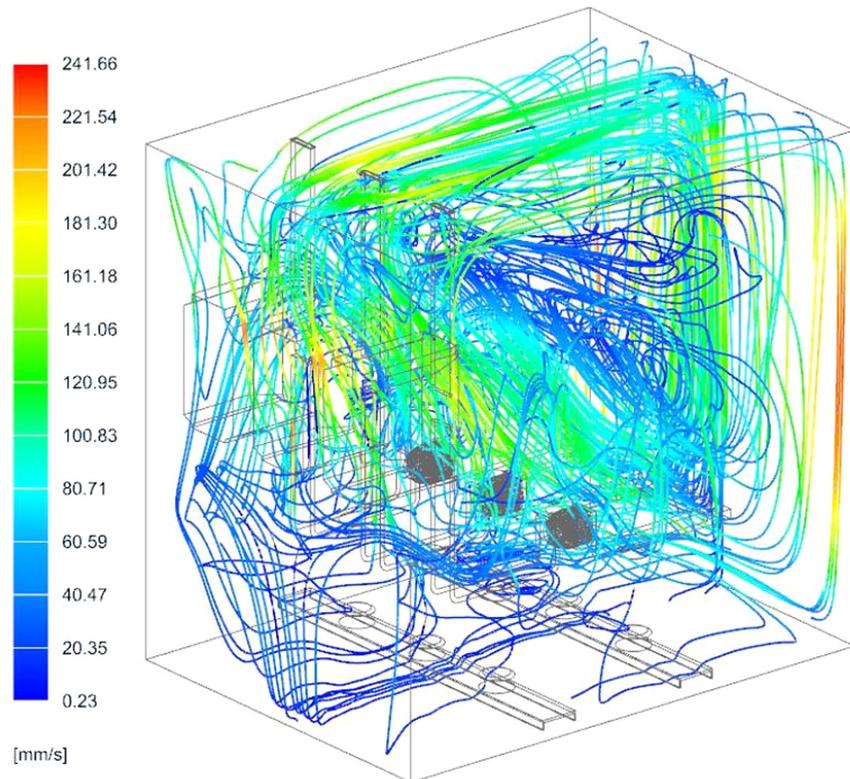

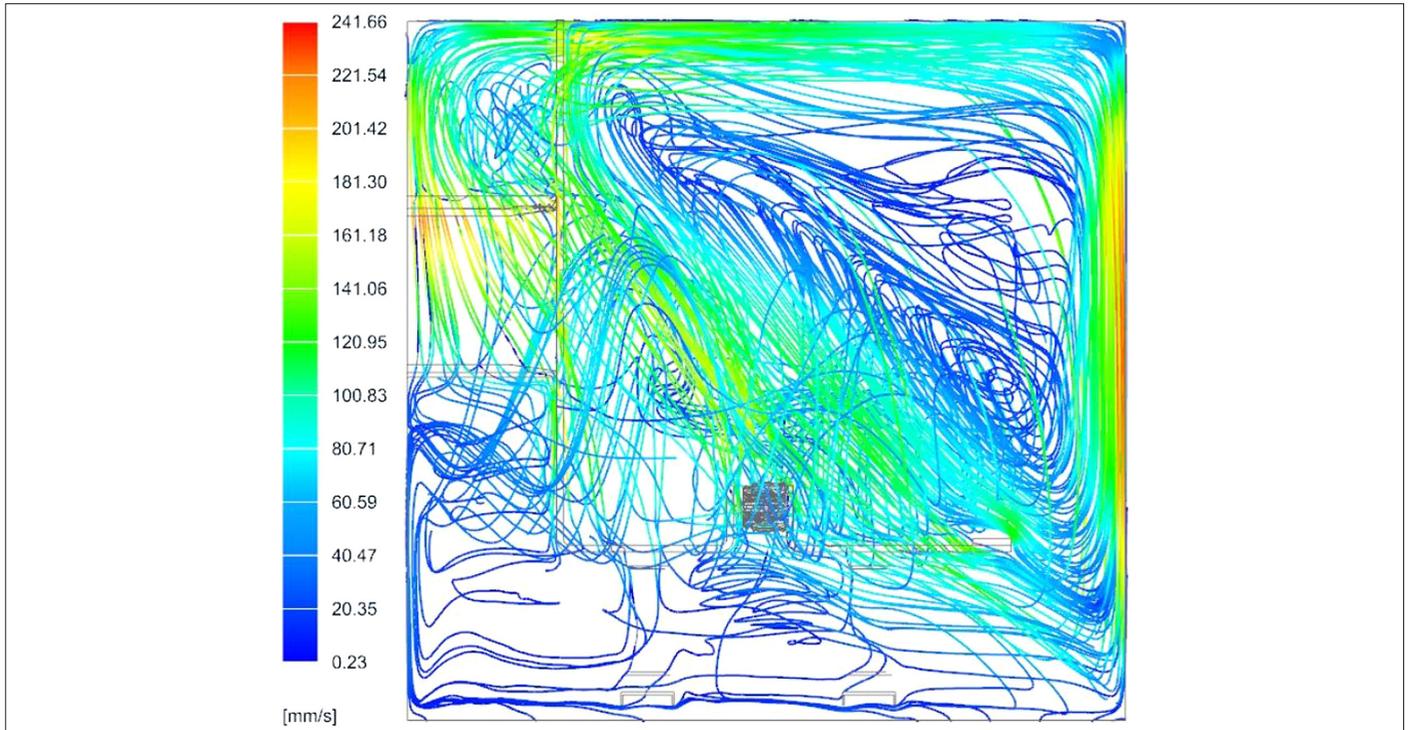**Fig. 12.** Velocity distribution of the computational model (three-dimensional view).

Fig. 13. Velocity distribution of the computational model (mid-section view).

In Section II, it is mentioned that the total power loss is 238.5 W. The summation of TECL obtained with fine mesh and TECL of the coils is 233.06 W. This value is nearly 2% discrepant from the experimental data. Accordingly, simulations and experiments show good agreement in the electrical domain. The temperature difference between the CFD analysis and the first experiment set is 17.8% in maximum. In the second set, higher temperatures were measured except for the third measurement point. Therefore, the temperature difference between the CFD analysis and the second experiment set is 20.6% in maximum. In the conference proceeding [14], heating caused by windings of the CTs was omitted and the temperature difference between experiment and simulation
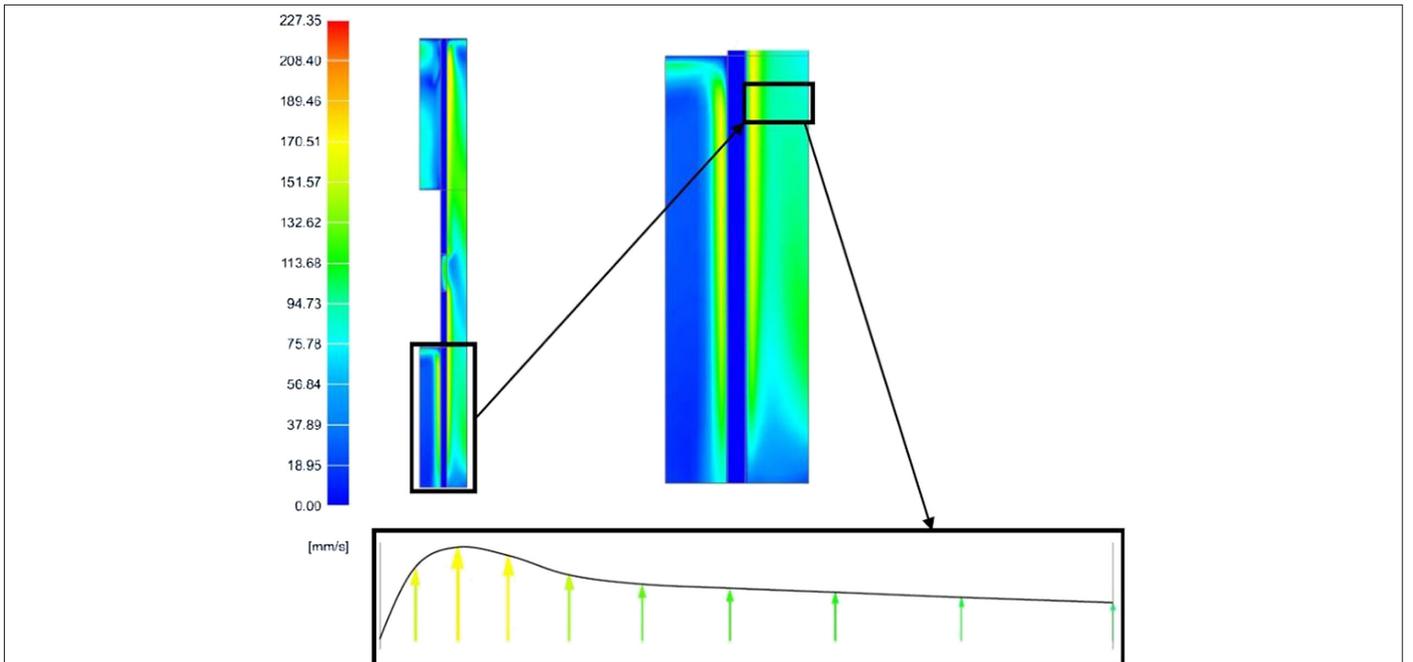

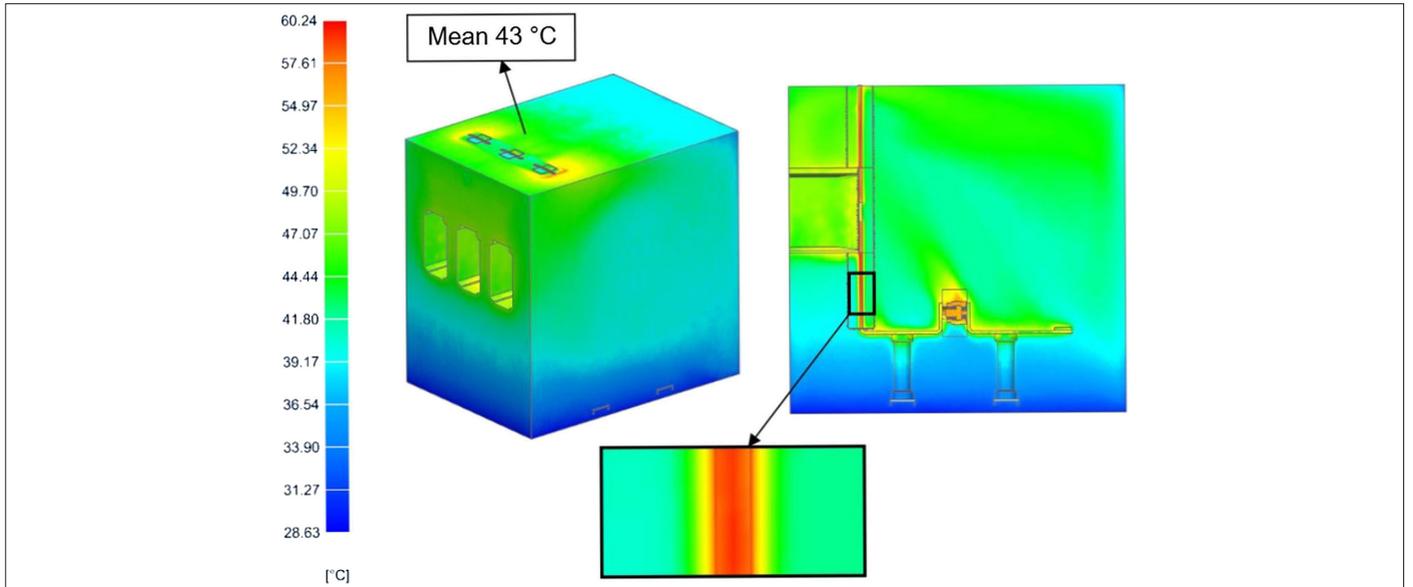**Fig. 14.** Velocity gradient in the boundary layer.

Fig. 15. Air temperature distribution of the computational model.

was about 26%. Implementing these heat sources to the system had a positive effect on the results. The calculated temperature values are in better agreement with the temperatures measured in the experiments, especially near the CTs. The main reason for the discrepancy between the temperature rise experiment sets is the lack of using the same ambient temperature. On the other hand, the measurement accuracy of the experimental setup should be considered.

TABLE VI. COMPARISON OF THE CALCULATED TEMPERATURES WITH DIFFERENT MESH DENSITIES

Mesh	C				M	F			
Number of elements	1 616 319				2 289 390	3 305 701			
Number of nodes	436 434				546 378	711 786			
Measurement Point	Temperature (°C)			Maximum Error Percentage	Measurement Point	Temperature (°C)			Maximum Error Percentage
	C	M	F			C	M	F	
TC_{R_1}	52.6	52.6	52.6	0	TC_{R_5}	55.2	55.6	56.0	1.43
TC_{S_1}	52.4	52.4	52.4	0	TC_{S_5}	55.9	56.3	56.5	1.06
TC_{T_1}	55.4	55.4	55.4	0	TC_{T_5}	55.1	55.5	55.8	1.25
TC_{R_2}	59	59	58.9	0.17	TC_{R_6}	55.1	55.5	55.9	1.43
TC_{S_2}	59	58.9	58.7	0.51	TC_{S_6}	55.8	56.2	56.5	1.24
TC_{T_2}	59.5	59.5	59.3	0.34	TC_{T_6}	55	55.4	55.7	1.26
TC_{R_3}	60.2	60.2	60.2	0	TC_{R_7}	55.1	55.4	55.8	1.25
TC_{S_3}	60.3	60.2	59.9	0.67	TC_{S_7}	55.8	56.1	56.4	1.06
TC_{T_3}	60	60	59.9	0.17	TC_{T_7}	55	55.3	55.7	1.26
TC_{R_4}	59.9	60.2	60.1	0.33	TC_{R_8}	55.5	55.7	56.4	1.6
TC_{S_4}	60.2	60.3	60.0	0.5	TC_{S_8}	55.6	55.8	56.3	1.24
TC_{T_4}	59.6	59.8	59.8	0.33	TC_{T_8}	55.5	55.7	56.2	1.25

C, coarse; M, medium; F, fine.

V. CONCLUSIONS

Analyses were performed in one-way coupled fashion. Namely, temperature dependency of electrical properties is neglected. Therefore, some of the power losses are still absent in the analysis results. Future work would be the two-way coupled simulation of the present computational model. Neglecting temperature changes causes smaller skin depth and bigger resistivity. While the former has a reducing effect on the power loss and hence temperature, the latter has an increasing effect on them. Increase in resistivity has a more significant effect on power losses than the skin depth. Hence, with a two-way coupled model, TECL can be expected to be greater than the current EMAG analysis results. Moreover, temperature values might be expected closer to experimental results due to the increase in the temperatures.

REFERENCES

1. M. Kazimierczuk, *High-Frequency Magnetic Components*. Chichester: Wiley, 2014.
2. A. Seker, *Modeling and thermal analysis of simplified medium voltage switchgear using computational methods*. M.Sc. National Defense University, 2020. Available: https://tez.yok.gov.tr/UlusalTezMerkezi/TezGoster?key=_F5QEpayDXGqGZlp9XiFtOTDFUWAXxmqXyV-vvKvoOnZm2C46cuc4oaWtCuUJMbKe
3. T. Radeva, I. Yatchev, D. Karastoyanov, N. Stoimenov, and S. Gyoshev, "Coupled electromagnetic and thermal field modeling of a laboratory busbar system," *Int. J. Electr. Comput. Eng.*, 2014. **[CrossRef]**
4. M. Bedkowski et al., "Coupled numerical modelling of power loss generation in busbar system of low-voltage switchgear," *Int. J. Therm. Sci.*, vol. 82, pp. 122–129, 2014. **[CrossRef]**
5. M. Bedkowski, J. Smolka, Z. Bulinski, A. Ryfa, and M. Ligeza, "Experimentally validated model of coupled thermal processes in a laboratory switchgear," *IET Gener. Transm. Distrib.*, vol. 10, no. 11, pp. 2699–2709, 2016. **[CrossRef]**
6. M. Bedkowski, J. Smolka, Z. Bulinski, and A. Ryfa, "Simulation of cooling enhancement in industrial low-voltage switchgear using validated coupled CFD-EMAG model," *Int. J. Therm. Sci.*, vol. 111, pp. 437–449, 2017. **[CrossRef]**
7. J. Qu, F. Chong, G. Wu, X. Li, and Q. Wang, "Application of computational fluid dynamics to predict the temperature-rise of low voltage switchgear compartment." 60th Holm Conference on Electrical Contacts (Holm). IEEE Publications, 2014. **[CrossRef]**
8. X. Zheng *et al.*, "Optimization on airflow distribution for anti-condensation of high-voltage switchgear using CFD method," *Case Stud. Therm. Eng.*, vol. 28, p. 101479, 2021. **[CrossRef]**
9. X. Guan, N. Shu, and H. Peng, "LBM simulation of heat transfer processes inside GIS capsule filled with different insulation gas mixtures," *Math. Comput. Simul.*, vol. 188, pp. 212–225, 2021. **[CrossRef]**
10. C. Gramsch, A. Blaszczyk, H. Löbl, and S. Grossmann, "Thermal network method in the design of power equipment," *Sci. Comput. Electr. Eng.*, pp. 213–219, 2007. **[CrossRef]**
11. X. Dong, R. Summer, and U. Kaltenborn, "Thermal network analysis in MV GIS design." IET Conference Publications, 2009. **[CrossRef]**
12. S. Singh, R. Summer, and U. Kaltenborn, "A novel approach for the thermal analysis of air insulated switchgear, CIRED." 21st International Conference on Electricity Distribution. Germany: Paper Publications, 2011, p. 0492.
13. R. Nowak, J. Duc, B. Samul, and A. P. Manjunatha, "A thermal network approach for a quick and accurate study of multiple connected switchgears," *Heat Transf. Eng.*, vol. 43, no. 3–5, pp. 183–197, 2022. **[CrossRef]**
14. A. Seker, E. Sakaci, A. Deniz, B. Celik, and D. Yildirim, "Thermal analyses for a simplified medium-voltage switchgear: Numerical and experimental benchmark studies." 11th International Conference on Electrical and Electronics Engineering (ELECO), 2019. **[CrossRef]**
15. High-Voltage Switchgear and Controlgear - Part 1: Common Specifications for Alternating Current Switchgear and Controlgear, IEC 62271-1:2017, 2017.
16. *Magnetics for NX, Dr. Binde Ingenieure*. Design & Engineering GmbH. Available: https://magnetics.de.
17. R. Anderl, and P. Binde, *Simulations with NX*. Cincinnati: Hanser Publications, 2018.
18. European Commission, "Online material characterisation at strip production," 2013. Available: http://www.gotrawama.eu/siderurgia/Online%20material%20characterisation%20at%20strip%20production%20(OMC).pdf.
19. H. Tran-Cor, "Grain oriented electrical steels." Available: https://www.aksteel.eu/files/downloads/TRAN-COR_H_%20Grain_Oriented_Electrical_Steel.pdf.
20. F. P. Incropera, and D. P. DeWitt, *Fundamentals of Heat and Mass Transfer*, 4th ed. Hoboken: Wiley, 1996.
21. *Flow Solver Reference Manual*. Siemens, 2017 Available: https://docs.plm.automation.siemens.com/data_services/resources/nx/12/nx_help/common/en_US/graphics/fileLibrary/nx/tdoc_advanced_simulation/flowrefman.pdf.

Ahmet Efe Seker received his B.Sc. degree in Mechanical Engineering from Faculty of Engineering, Karadeniz Technical University, Turkey, in 2015. He received his M.Sc. degree in Aeronautical Engineering from National Defense University, Turkey, in 2020. He is currently a Ph.D. student at Istanbul Technical University, Aeronautical and Astronautical Engineering Program.

Bayram Celik received his B.Sc. degree in Astronautical Engineering from Faculty of Aeronautical and Astronautical Engineering, Istanbul Technical University, Turkey, in 1993. He received his M.Sc. and Ph.D. degree in Aeronautical and Astronautical Engineering from Istanbul Technical University, Turkey, in 1997 and 2006, respectively. He is currently working at Istanbul Technical University as Associate Professor.

Deniz Yildirim was born in Istanbul, Turkey. He received BS degree in Electrical Engineering from Istanbul Technical University in 1989 and MS and PhD degrees in Electrical Engineering from University of Colorado at Boulder in 1993 and 1999, respectively.

His research areas include power converters, electrical machines, and utility interactions of renewable energy (solar and wind power) sources. He has various industial consulting experience in industry regarding FEM analysis, solar potential calculation, electronic circuit design, inverters, and electromechanical component designs. He is currently an Assistant Professor of Electrical Engineering in Istanbul Technical University, Istanbul, Turkey.

Egemen Aslan Sakaci received his B.Sc. degree in Mechanical Engineering Department from Middle East Technical University, Ankara, Turkey in 2009. He is currently working for Siemens, Turkey, as Expert Research and Development Engineer. His major research interest areas are mechanical design and engineering simulations.

Arif Deniz received his B.Sc. degree in Mechanical Engineering from Faculty of Engineering, Istanbul Technical University, Turkey, in 2002. He has been working as a Senior Engineer at Siemens Gebze R&D Center, Turkey, since 2009. His main area of expertise is the design, testing, and analysis of requirements for standard and non-standard medium-voltage switchgears.